Self-trapped magnetic polaron in electron-doped $CaMnO_3$

2005 J. Phys.: Condens. Matter 17 1889

(http://iopscience.iop.org/0953-8984/17/12/013)

INSTITUTE OF PHYSICS PUBLISHING JOURNAL OF PHYSICS: CONDENSED MATTER

J. Phys.: Condens. Matter **17** (2005) 1889–1906 doi:10.1088/0953-8984/17/12/013

Self-trapped magnetic polaron in electron-doped $CaMnO_3$

H Meskine and S Satpathy

Department of Physics and Astronomy, University of Missouri-Columbia, Columbia, MO 65211, USA

Received 11 October 2004, in final form 1 February 2005
Published 11 March 2005
Online at stacks.iop.org/JPhysCM/17/1889

Abstract

We study the energetics of the self-trapped magnetic polaron (electron plus the distorted local magnetization cloud) in electron-doped manganites, e.g., $Ca_{1-x}La_xMnO_3$, with small x and at zero temperature. A single electron moving in a cubic lattice of antiferromagnetic t_{2g} core spins, as appropriate for the manganites, is examined, taking into account the effects of the nearest- and the next-nearest-neighbour hoppings and the Anderson–Hasegawa double-exchange, as well as the Jahn–Teller interaction. We compute the ground-state energy and the wavefunction of the system using a set of self-consistent equations. While we show that the next-nearest-neighbour hopping significantly reduces the binding energy of the magnetic polaron, this reduction is not enough to destabilize the self-trapped state. The ground state of the polaron is found to be a seven-site ferromagnetic region, comprising the central spin and the six nearest neighbours, with a net magnetic moment of approximately 7 μ_B, in qualitative agreement with the interpretation of Neumeier and Cohn of their experimental magnetization data (Neumeier and Cohn 2000 *Phys. Rev.* B **61** 14319). We argue that the polaron should exhibit an activated hopping as seen in the experiments, and estimate an activation energy of about 40 meV.

1. Introduction

It is well established that an electron in a polar material becomes dressed with a cloud of lattice distortions (phonons) as it travels through the solid, forming the lattice polaron or simply the polaron. The underlying electron–phonon interaction manifests itself in a number of effects such as the enhancement of the electron mass as well as the specific heat, and leads to a host of phenomena, notably the phonon-mediated superconductivity.

In an analogous manner, an electron in a magnetic solid can distort the local moment due to the interaction between the spin of the electron and the magnetic moments of the local ions. The electron becomes dressed with a magnetic polarization cloud; they travel together as a unit

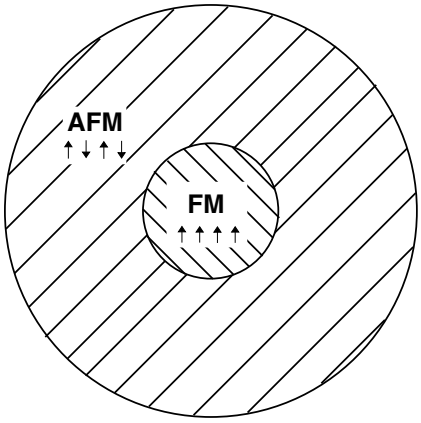

Figure 1. Sketch of a self-trapped magnetic polaron, where the electron nucleates an exchange-induced ferromagnetic core in the middle of an antiferromagnetic lattice. The electron becomes trapped in the magnetic potential well of the ferromagnetic region.

in the solid. This is called the magnetic polaron. While the concept has been formulated quite early on since the 1970s through the seminal works of Nagaev, Mott, Kasuya, and a host of other authors [2–4], the magnetic polaron remains a relatively unstudied entity. This is because the relatively weak magnetic coupling that underlies the formation of the magnetic polaron leads to a much smaller effect as compared to the lattice polaron, where the underlying interaction is the strong Coulomb force. The phenomenon has nevertheless been well documented in the magnetic semiconductors, where it leads to a number of novel effects such as the giant red shifts in the band gap and the spectacular metal–insulator transition in EuO [5–7]. The emerging interest in transport in magnetic materials for spintronic applications, for example, the dilute magnetic semiconductors such as GaAs(Mn), has renewed interest in the study of the magnetic polarons.

Figure 1 shows a sketch of a magnetic polaron consisting of an itinerant electron plus a local ferromagnetic (FM) region that it nucleates via the exchange interaction in an otherwise antiferromagnetic lattice of local spins. A distinction is made between the bound magnetic polaron, where the electron is bound to a defect centre and polarizes the localized magnetic moments in its neighbourhood, and the self-trapped magnetic polaron, where the electron is trapped in the magnetic potential well that it produces via the exchange interaction with the local moments. Analogous to the case of the lattice polaron, the magnetic polaron must carry the magnetic distortion along with it, as it moves from site to site in the lattice. There are important differences in the conduction properties of the bound magnetic polaron and self-trapped magnetic polaron. While the bound magnetic polaron should always show activated conductivity, the self-trapped magnetic polaron should have metallic conductivity in the weak coupling limit, with a modified effective mass, and presumably an activated conductivity in the strong coupling limit.

The giant red shifts in the band gap and the metal–insulator transition in certain materials such as EuO have been explained in terms of the bound magnetic polaron. In contrast, while the self-trapped magnetic polaron is believed to exist in antiferromagnetic (AF) semiconductors such as EuSe and EuTe as well as in Gd-doped $Eu_{1-x}Gd_xSe$ and $Eu_{1-x}Gd_xTe$ [8–11], its existence is however not conclusively established. Recent experiments [1] have suggested the existence of the self-trapped magnetic polaron in the manganites, where measurements of the saturation magnetization of $Ca_{1-x}La_xMnO_3$ at low doping levels ($x \leqslant 0.07$) are consistent

with the presence of local FM regions in the globally AF lattice. This was attributed by the authors to the stabilization of a self-trapped magnetic polaron state in low electron-doped $CaMnO_3$.

It is the purpose of this work to study the energetics and the formation of the self-trapped magnetic polaron in $Ca_{1-x}La_xMnO_3$ in the light doping limit, taking into account the coupling between the electronic, lattice, and the spin degrees of freedom. A variational approach is adopted to study the ground state of the system within our model, the results of which are compared to selected density-functional calculations.

Our conclusions may be summarized as follows.

(1) We find that the Jahn–Teller interaction increases the binding energy of the self-trapped magnetic polaron only marginally, while the second-neighbour hopping has an opposite and a much larger effect.
(2) Although the second-neighbour hopping reduces the polaron binding drastically, the reduction is nevertheless not strong enough to destabilize the polaron entirely.
(3) For parameters appropriate for the manganites, the polaron binding energy is in the range of 100 meV or so, while the configuration of the lattice spins is generally a seven-site ferromagnetic cluster (central site plus the six nearest neighbours on the cubic lattice), formed by flipping the central spin. The lattice spin configuration is consistent with the experimental observation [1] as well as earlier theoretical work of Chen and Allen [12].
(4) And, finally, we suggest why the self-trapped magnetic polaron in electron-doped $CaMnO_3$ should show an activated conductivity and we estimate this activation energy to be less than the polaron binding energy, but only by a small amount.

The paper is organized as follows. In section 2 we discuss the basic physics of the self-trapped magnetic polaron within the simple model of Mott. Section 3 introduces a model Hamiltonian appropriate to the magnetic polaron in $CaMnO_3$. Section 4 describes the method of calculation, with the results discussed in section 5, followed by a summary in section 4.

2. The Mott polaron

Before studying the magnetic polaron in $CaMnO_3$, we discuss the Mott model which, despite its simplicity, captures many features of the magnetic polaron physics. We consider an AF lattice where the fixed lattice spins interact through an antiferromagnetic Heisenberg-like exchange of the form $J\boldsymbol{S}_i \cdot \boldsymbol{S}_j$ ($J > 0$ is the exchange coupling constant). When a single excess electron of mass m is introduced into the AF lattice, it will interact with the spins of the lattice via a ferromagnetic interaction. This interaction will tend to polarize an FM region around the site occupied by the excess electron (see figure 1).

Mott considered the magnetic polaron to consist of a saturated ferromagnetic region of radius R (the polaron radius), with the rest of the lattice being antiferromagnetic. In reality, there would be no such abrupt boundary as envisaged by Mott, but rather a gradual change between the FM and the AF regions [13]. In spite of this deficiency, Mott's idea of the magnetic polaron remains a simple yet powerful way to think of the problem.

In Mott's picture, the size of the polaron is determined by a competition between the superexchange between the localized spins, which favours the antiferromagnetic lattice, and the kinetic energy of the electron which favours a ferromagnetic region. If the energy cost to turn a single bond from AF to FM is $2JS^2$ (the energy of the AF bond is by convention zero), then the exchange energy cost to form the ferromagnetic region of radius R is $(\nu/2) \times 2JS^2 \times \frac{4\pi}{3}(R/a)^3$, where a is the lattice constant and ν is the number of nearest neighbours. Assuming an infinite Hund's coupling, the electron is forbidden to leave the FM region and becomes trapped inside

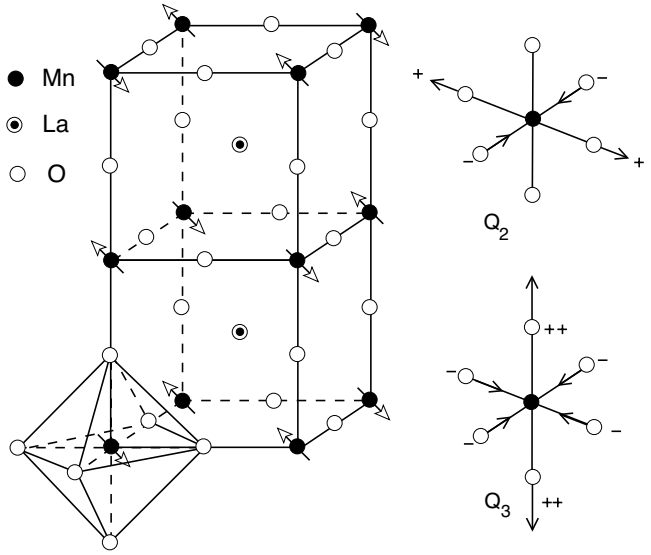

Figure 2. Type-G magnetic structure of $CaMnO_3$ and the normal modes of the MnO_6 octahedron, to which the e_g electrons couple via the Jahn–Teller effect.

an infinite potential well with the particle-in-a-box confinement energy $\hbar^2\pi^2/2mR^2$. The energy of the system then reads

$$E = -\nu|t| + \frac{\hbar^2\pi^2}{2mR^2} + \nu JS^2\frac{4\pi}{3}\left(\frac{R}{a}\right)^3, \tag{1}$$

where $-\nu|t|$ is the energy of the band bottom for the electron moving in a completely ferromagnetic lattice and t is the nearest-neighbour hopping integral.

The electron mass m at the band bottom is related to the tight-binding integral via the expression $\hbar^2/m = |t|a^2$. The polaron energy E_{Mott} is obtained by minimizing the expression (1) as a function of the polaron radius R, which yields

$$\begin{aligned} R &= \left(\frac{\pi\alpha}{4\nu}\right)^{1/5} a, \\ E_{\mathrm{Mott}}/|t| &= A\alpha^{-2/5} - \nu, \end{aligned} \tag{2}$$

where $\alpha = |t|/JS^2$ and A is a numerical constant. The binding energy of the magnetic polaron is the energy gained over that of the AF lattice:

$$E_{\mathrm{B}} = E_{\mathrm{AF}} - E_{\mathrm{Mott}}. \tag{3}$$

For parameters appropriate to $CaMnO_3$ [14–16], $|t| = 0.5$–0.75 eV, and $JS^2 = 5$ meV, the polaron radius is $R \approx 1.8a$, with a binding energy E_{B} which varies between 0.03 and 0.38 eV and increases as a function of t.

Jahn–Teller coupling—Consider now the effect of the Jahn–Teller coupling on the Mott polaron. In $CaMnO_3$ which forms in the perovskite structure, six oxygens form an octahedron around the manganese ion with the Mn^{4+} valence (figure 2). When an excess electron is added to the manganese, thus changing the valence from Mn^{4+} to Mn^{3+}, the MnO_6 octahedra will distort in order to lower the energy of the system via the Jahn–Teller effect. In $CaMnO_3$ the Jahn–Teller coupling is of type $e \otimes E$, coupling the e_g electrons to the E_g normal modes of

the isolated single octahedron. The Hamiltonian describing this coupling reads [17, 18]

$$H_{\mathrm{JT}} = \frac{K}{2}\sum_{i=1}^{3} Q_i^2 - g(\sigma_x Q_2 + \sigma_z Q_3), \tag{4}$$

where Q_1, Q_2, and Q_3 are, respectively, the breathing mode, and the in-plane and the apical stretching modes of the isolated MnO_6 octahedron (figure 2), and σ is the pseudo-spin describing the two e_g orbitals, $|\uparrow\rangle = |z^2 - 1\rangle$ and $|\downarrow\rangle = |x^2 - y^2\rangle$. The lattice stiffness and electron–lattice coupling constants are denoted K and g, respectively.

For an isolated octahedron with one e_g electron present, the energy gain caused by the Jahn–Teller coupling is well known [19]. Diagonalization of the 2×2 Hamiltonian (4) leads to the 'Mexican hat' potential surface:

$$E = \tfrac{1}{2} K Q^2 \pm g Q, \tag{5}$$

where $Q \equiv (Q_2^2 + Q_3^2)^{1/2}$, and since the Jahn–Teller coupling as seen from equation (4) does not contain the Q_1 distortion, we have suppressed it. The equation represents the competition between the elastic energy and the one-particle electronic energy. For the ground state, where the electron occupies the lower of these two potential surfaces, the distortion corresponding to the energy minimum is given by $Q = g/K$, which results in the Jahn–Teller energy gain $E_{\mathrm{JT}} = -g^2/2K$.

The above expression for E_{JT} was derived for a single octahedron, but obviously, it is also valid for the solid provided that the electron is restricted to a single octahedron, as would be the case if the electron hopping is prohibited between the octahedra (for instance, for the AF arrangement of the Mn moments in the nearest-neighbour model with 1NN hopping suppressed via double exchange). For the more general case, the electron is spread over several octahedra.

We now proceed to estimate the E_{JT} in the case of a solid, where the electron is spread over several octahedra, which is generally the case. We have to consider each octahedron separately. The second term in equation (5) representing the electronic energy gain for a specific octahedron has to be multiplied by the electron occupancy for that octahedron. This 'dilutes' the effect of the Jahn–Teller coupling.

The energy gain may be estimated by putting a fractional number of electrons at each octahedral site in the following manner. If $n(r)$ is the occupancy of the electron at the octahedron at the position r, then the energy surface controlling the octahedral distortion is, analogously to equation (5), given by

$$E(r) = \frac{K}{2} Q(r)^2 \pm g\, Q(r) n(r), \tag{6}$$

where the octahedral distortion $Q(r)$ is now position dependent. The minimum occurs at $Q(r) = (g/K) \times n(r)$ with the corresponding energy gain

$$E_{\mathrm{JT}}(r) = -\frac{g^2}{2K} n^2(r). \tag{7}$$

The electron density $n(r)$ at site r is calculated from the particle-in-a-box ground-state wavefunction

$$\psi(r) = \left(\frac{\pi}{2R^3}\right)^{1/2} j_0\left(\frac{\pi r}{R}\right) = \left(\frac{1}{2\pi R}\right)^{1/2} \frac{\sin(\pi r/R)}{r}, \tag{8}$$

where $j_0(x)$ is the spherical Bessel function of 0th order. Considering a spherical shell of radius r and thickness $\mathrm{d}r$, the number of MnO_6 octahedra in this shell is $(4\pi r^2\,\mathrm{d}r)/a^3$, with the electron occupancy of each octahedron being $n(r) = a^3\,|\psi(r)|^2$. The correction to the

Mott energy due to the Jahn–Teller distortion is then

$$\begin{aligned} E_{\mathrm{JT}} &= \int_0^R E_{\mathrm{JT}}(r)\,\mathrm{d}r \\ &= -\int_0^R \frac{g^2}{2K} n^2(r) \frac{4\pi r^2}{a^3}\,\mathrm{d}r \\ &= -\frac{g^2}{2K} c_0 \left(\frac{a}{R}\right)^3, \end{aligned} \tag{9}$$

where c_0 is a numerical constant:

$$c_0 = \int_0^\pi \frac{\sin^4 x}{x^2}\,\mathrm{d}x \approx 0.6721. \tag{10}$$

Clearly, this analysis assumes a large polaron limit, while the polaron size in the manganites is rather small, extending over a region of just a couple of lattice constants. One may not therefore expect to obtain a good estimate from this calculation. Nevertheless, the energy estimated from this crude approach is rather good, as seen from the results presented in the later part of this paper, justifying *a posteriori* the large polaron limit here.

Adding the Jahn–Teller energy gain from equation (9), the Mott expression equation (1) for the polaron energy becomes

$$E = E_{\mathrm{bottom}} + \frac{\hbar^2\pi^2}{2mR^2} + \nu J S^2 \frac{4\pi}{3}\left(\frac{R}{a}\right)^3 - \frac{g^2}{2K} c_0 \left(\frac{a}{R}\right)^3. \tag{11}$$

We have taken a nearest-neighbour tight-binding two-bands model for the e_g electrons on a cubic lattice with the hopping integral $t = V_{dd\sigma}$, so that the band structure is given by

$$\begin{aligned} E(\boldsymbol{k})/t = \cos k_x a + \cos k_y a + \cos k_z a \pm [&\cos^2 k_x a + \cos^2 k_y a + \cos^2 k_z a \\ &- \cos k_x a \cos k_y a - \cos k_y a \cos k_z a - \cos k_z a \cos k_x a]^{1/2}. \end{aligned} \tag{12}$$

It can be easily shown that, with this band structure, the energy of the bottom band and effective mass are given by $E_{\mathrm{bottom}} = -3|t|$ and $\hbar^2/m = (3/2)|t|a^2$, respectively.

Figure 3 shows the energy as a function of the polaron radius for several values of the dimensionless coupling constant Γ defined as $\Gamma = g^2/(K|t|)$. The solid curve corresponds to the parameters appropriate for $CaMnO_3$ (with $g = 2$ eV Å^{-1}, and $K = 10$–20 eV Å^{-2}) and its minimum gives the polaron energy and the polaron radius R ($R \lesssim 2a$ in the figure). These values are very close to the ones found without the Jahn–Teller effect, suggesting that the Jahn–Teller coupling does not affect the polaron energy significantly for the systems under study. The dashed curve shows the Mott energy for a much larger value of Γ. The total energy is lowered by the Jahn–Teller gain $E_{\mathrm{JT}} \approx (g^2 c_0/2K)(a/R)^3$, while the radius of the polaron region is slightly reduced by the Jahn–Teller interaction.

3. Hamiltonian for the magnetic polaron

The basic electronic structure of the manganites is illustrated in figure 4, where the results of the local-spin-density-functional studies for the antiferromagnetic $CaMnO_3$ have been summarized in the form of a one-electron density-of-states. Doping with La introduces electrons into the unoccupied e_g band, which form the itinerant electrons, able to hop from site to site in a lattice of t_{2g} spins. A single excess electron introduced in the system through light doping will thus occupy the lowest e_g orbital, with its spin parallel to that of the t_{2g} electrons, and will cause the degeneracy of the e_g orbitals to be lifted via the Jahn–Teller effect [20].

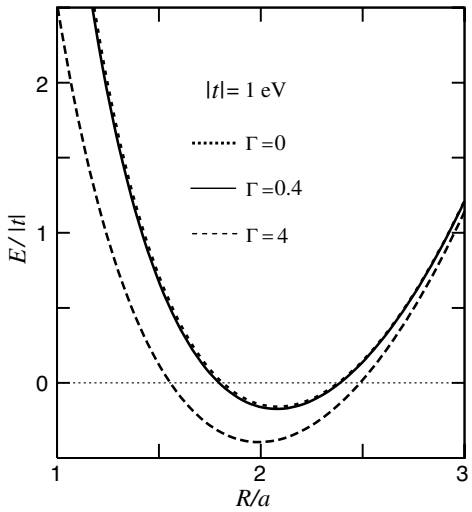

Figure 3. The total energy of the Mott polaron with the Jahn–Teller interaction included in the large polaron limit (following equation (11)). The Jahn–Teller interaction increases the binding energy of the magnetic polaron somewhat, while at the same time reducing its size.

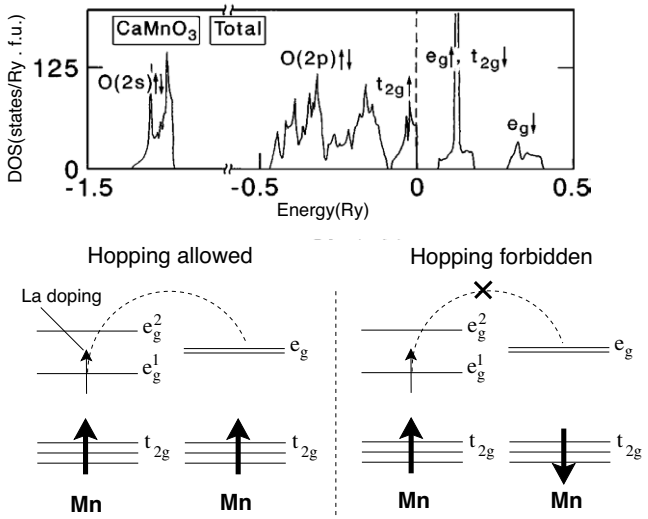

Figure 4. Density of states for antiferromagnetic $CaMnO_3$ as obtained from density-functional calculations [21]. The dashed curve indicates the position of the Fermi energy. Electrons introduced via La doping occupy the $e_g\uparrow$ conduction band, moving in a lattice of localized t_{2g} moments. The lower part of the figure illustrates the physics of the Anderson–Hasegawa double exchange, in which hopping of an itinerant e_g electron is forbidden to a site if the t_{2g} spin at that site is aligned in the opposite direction. This is strictly true if the Hund's rule energy cost is infinity.

The Hamiltonian describing the motion of the itinerant electron in the lattice consists of three parts,

$$\mathcal{H} = \mathcal{H}_{\rm el} + \mathcal{H}_{\rm ex} + \mathcal{H}_{\rm JT}, \tag{13}$$

which are, respectively, the electronic kinetic energy, the superexchange between the t_{2g} spins, and the Jahn–Teller coupling terms.

Table 1. The Koster–Slater hopping matrix elements between nearest- and next-nearest-neighbours e_g orbitals as calculated in [23]. $|e_g^1\rangle$ and $|e_g^2\rangle$ refer respectively to $|3z^2 - r^2\rangle$ and $|x^2 - y^2\rangle$ d states, while (V_σ, V_π) and (V'_σ, V'_π) are the first- and second-neighbour tight-binding hopping parameters.

Direction	$\langle e_g^1\|H_{el}\|e_g^1\rangle$	$\langle e_g^1\|H_{el}\|e_g^2\rangle$	$\langle e_g^2\|H_{el}\|e_g^2\rangle$
$\hat{x}$	$\frac{1}{4}V_\sigma$	$-\frac{\sqrt{3}}{4}V_\sigma$	$\frac{3}{4}V_\sigma$
$\hat{y}$	$\frac{1}{4}V_\sigma$	$\frac{\sqrt{3}}{4}V_\sigma$	$\frac{3}{4}V_\sigma$
$\hat{z}$	V_σ	0	0
$\hat{x}+\hat{y}$	$\frac{1}{4}V'_\sigma$	0	V'_π
$\hat{y}+\hat{z}$	$\frac{1}{16}V'_\sigma + \frac{3}{4}V'_\pi$	$\frac{\sqrt{3}}{16}V'_\sigma - \frac{\sqrt{3}}{4}V'_\pi$	$\frac{3}{16}V'_\sigma + \frac{1}{4}V'_\pi$
$\hat{z}+\hat{x}$	$\frac{1}{16}V'_\sigma + \frac{3}{4}V'_\pi$	$-\frac{\sqrt{3}}{16}V'_\sigma + \frac{\sqrt{3}}{4}V'_\pi$	$\frac{3}{16}V'_\sigma + \frac{1}{4}V'_\pi$

The first term is of the Anderson–Hasegawa form [22],

$$\mathcal{H}_{el} = \sum_{ij,\alpha\beta} t_{ij}^{\alpha\beta} \cos\frac{\theta_{ij}}{2} c_{i\alpha}^\dagger c_{j\beta} + \text{h.c.}, \tag{14}$$

which assumes an infinite Hund's rule energy, a reasonable approximation for the manganites, and considers explicitly only the Mn atoms on a cubic lattice. Here $c_{i\alpha}^\dagger$ ($c_{i\alpha}$) is the creation (annihilation) operator for the electron, with i being the site index and α being the orbital index corresponding to the two e_g orbitals ($z^2 - 1$ or $x^2 - y^2$ for $\alpha = 1$ or 2), with the electron spin parallel to the t_{2g} spin. This in effect renders the electron spinless, since it must be aligned to the local t_{2g} spin, a consequence of the infinite Hund's rule energy. $t_{ij}^{\alpha\beta}$ are the Koster–Slater matrix elements as expressed in table 1 and θ_{ij} is the angle difference between the spin angles θ_i and θ_j of two neighbouring t_{2g} spins:

$$\theta_{ij} = \theta_j - \theta_i. \tag{15}$$

There are three angle differences per each site i, corresponding to the three neighbours along the positive x, y, and z directions.

The second term in the Hamiltonian (13) is the antiferromagnetic superexchange between the t_{2g} spins,

$$\mathcal{H}_{ex} = J\sum_{\langle i,j\rangle} \boldsymbol{S}_i \cdot \boldsymbol{S}_j = JS^2 \sum_{\langle i,j\rangle} (1 + \cos\theta_{ij}), \tag{16}$$

where in writing down the last term, the spins have been taken to be classical and the zero of energy has been redefined such that the AF alignment of neighbouring spins has zero energy.

The last term in equation (13) is the electron–lattice coupling due to the Jahn–Teller effect:

$$\mathcal{H}_{JT} = \sum_i \frac{K}{2}(Q_{1i}^2 + Q_{2i}^2 + Q_{3i}^2) - g\,[\,c_{i1}^\dagger \quad c_{i2}^\dagger\,] \begin{pmatrix} Q_{3i} & Q_{2i} \\ Q_{2i} & -Q_{3i} \end{pmatrix} \begin{bmatrix} c_{i1} \\ c_{i2} \end{bmatrix}. \tag{17}$$

This is analogous to equation (4), except that now we sum over all sites in the lattice.

We introduce the nearest- and the next-nearest-neighbour hopping parameters $t_{1NN} = -V_{dd\sigma}$ and $t_{2NN} = -V'_{dd\sigma}$, whose values as estimated from the density functional calculations [15] are $t_{1NN} = 0.5$–0.75 eV and $t_{2NN} = 0.2$–0.3 eV. We use the Harrison scaling [23] $V'_{dd\pi} \approx -0.54V'_{dd\sigma}$ for the next-nearest-neighbours matrix elements. The remaining

parameters are the superexchange J, which is such that $JS^2 \approx 5$ meV [24–26], and the lattice stiffness and the Jahn–Teller coupling parameters may be estimated from the *ab initio* DFT calculations [14] of $LaMnO_3$ to be $K = 10$–20 eV Å^{-2} and $g = 2$ eV Å^{-1}.

4. Method of solution

The basic problem is to find the ground-state wavefunction of the excess electron and the corresponding spin and lattice distortions that minimize the expectation value of the energy for the Hamiltonian, equation (13). To this end, we write the ground state as a product function:

$$|\Psi\rangle = |\psi_e\rangle \otimes |Q\rangle \otimes |\theta\rangle \tag{18}$$

where $|Q\rangle$ and $|\theta\rangle$ denote the lattice distortions and the spin angles for the entire lattice, while $|\psi_e\rangle = \sum_{i\alpha} \psi_{i\alpha} c^{\dagger}_{i\alpha} |0\rangle$ describes the electronic wavefunction, where again i is the site index and α is the orbital index, running over the two e_g states.

In terms of the pseudo-spin operators σ_x and σ_z used to describe the two e_g orbitals, the energy corresponding to the Hamiltonian equation (13) is given by

$$E = \langle\Psi|H|\Psi\rangle = \sum_{ij}\sum_{\alpha\beta} t_{ij}^{\alpha\beta} \cos\frac{\theta_{ij}}{2} \psi^*_{i\alpha}\psi_{j\beta} + JS^2 \sum_{\langle i,j\rangle}(1+\cos\theta_{ij}) + \frac{K}{2}\sum_i Q_i^2 - g\sum_i\sum_{\alpha\beta}\psi^*_{i\alpha}\psi_{i\beta}\left(\sigma_x^{\alpha\beta}Q_{2i} + \sigma_z^{\alpha\beta}Q_{3i}\right). \tag{19}$$

The problem is then to find the global minimum of the total energy (19) as a function of the variational parameters ($\psi_{i\alpha}$, Q_{ij}, and θ_{ij}) subject to the normalization constraint for the wavefunction. This is accomplished by the usual Lagrange multiplier method:

$$F = E - \Lambda\left(\sum_{i\alpha} 1 - |\psi_{i\alpha}|^2\right), \tag{20}$$

where Λ is the Lagrange multiplier.

The conditions for the minimum energy are given by $\partial F/\partial\psi_{i\alpha} = 0$, $\partial F/\partial Q_{2i} = 0$, $\partial F/\partial Q_{3i} = 0$, and $\partial F/\partial\theta_i = 0$, which yield the following set of non-linear equations:

$$\sum_{j\beta} t_{ij}^{\alpha\beta}\cos\frac{\theta_i-\theta_j}{2}\psi_{j\beta} - \Lambda\psi_{i\alpha} - \sum_\beta g(\sigma_x^{\alpha\beta}Q_{2i} + \sigma_z^{\alpha\beta}Q_{3i})\psi_{i\beta} = 0 \tag{21}$$

$$KQ_{2i} - g\sum_{\alpha\beta}\sigma_x^{\alpha\beta}\psi^*_{i\alpha}\psi_{i\beta} = 0 \tag{22}$$

$$KQ_{3i} - g\sum_{\alpha\beta}\sigma_z^{\alpha\beta}\psi^*_{i\alpha}\psi_{i\beta} = 0 \tag{23}$$

$$A\sin\frac{\theta_i}{2} + C\sin\theta_i - B\cos\frac{\theta_i}{2} - D\cos\theta_i = 0 \tag{24}$$

where we have defined

$$A = \sum_j \varepsilon_{ij}\cos\frac{\theta_j}{2}, \qquad B = \sum_j \varepsilon_{ij}\sin\frac{\theta_j}{2}, \qquad C = \sum_j \varepsilon_{ij}\cos\theta_j, \qquad D = \sum_j \varepsilon_{ij}\sin\theta_j \tag{25}$$

with $\varepsilon_{ij} = \sum_{\alpha\beta} t_{ij}^{\alpha\beta}\psi^*_{i\alpha}\psi_{j\beta}$.

The above set of coupled equations is then solved self-consistently by taking an initial guess for the angles θ and then computing the lattice distortions Q_2 and Q_3 followed by

the wavefunction ψ at each step. New angles θ are then computed by finding the roots of equation (24). We take a large number of initial guesses to ensure convergence to a global minimum.

The binding energy E_B of the magnetic polaron is defined as the energy gained in forming a magnetic polaron state over the type-G AF arrangement of the t_{2g} spins:

$$E_B = E_{AF} - E_P. \tag{26}$$

The AF energy E_{AF} is calculated as the ground-state energy of the system with fixed t_{2g} spins in the AF type-G configuration. This amounts to solving equations (21)–(24) with the fixed spin angles θ, while the polaron energy E_P is found from the same set of equations with the spin angles allowed to vary.

5. Results

5.1. Formation of the magnetic polaron

The basis physics of the formation of the magnetic polaron is that the electron induces a ferromagnetic region so that it is delocalized over that region, reducing its kinetic energy. Before we present the results of the full calculation, it is instructive to examine this effect for the electron-doped $CaMnO_3$ in a simple model.

To this end, we consider the motion of an e_g electron in a cubic lattice of fixed t_{2g} spins, which do not have any degrees of freedom, but merely modify the e_g electron hopping via the Anderson–Hasegawa $\cos\theta/2$ factor. Also, no lattice distortions are allowed and only the 1NN and 2NN hopping integrals are retained, so that the tight-binding electronic Hamiltonian, equation (14), describes the e_g electrons in the system.

We consider two cases: one, where the t_{2g} spins form an antiferromagnetic cubic lattice and the other, where just one t_{2g} spin is flipped from the previous case, so that a seven-site (central Mn and its six nearest neighbours) FM region is formed.

The energy-resolved e_g electron density of states for the fully AF cubic lattice is shown as the solid curve in figure 5. Note that in this case, the Anderson–Hasegawa $\cos\theta/2$ factor completely suppresses the 1NN hopping, so that the band-width comes just from the 2NN hopping. Now, in the second case, with the seven-site FM region, the electron is allowed to hop to its first NNs as well within this limited FM region. Thus the two-fold e_g states belonging to the central site of the cluster gain a large kinetic energy (of the order of several t_{1NN}) and appear as split-off states below the band continuum, as indicated by the dashed lines in figure 5.

An added electron will occupy the e_g^1 state which has the lowest energy as shown in figure 4. This state is a combination of $3z^2 - r^2$ and $x^2 - y^2$ states, the particular mixture depending on the parameters. It is clear that if the ferromagnetic region is expanded, then the kinetic energy gain of the added electron will be even more. However, there is an energy cost of $2JS^2$ for a 'wrong' FM bond, so that the size of the FM region is determined by a balance between these two competing energy terms.

5.2. Effect of the Hamiltonian parameters on the polaron energy

An important point of this section is that the second-nearest-neighbour hopping t_{2NN} has a major effect on the energy of the polaron, although generally speaking, t_{2NN} is several times smaller than t_{1NN}, justifying the neglect of it in the tight-binding models.

The drastic effect of the second-nearest-neighbour hopping on the polaron energy is illustrated in figure 6, an effect that is quite easy to understand. Consider the extreme case

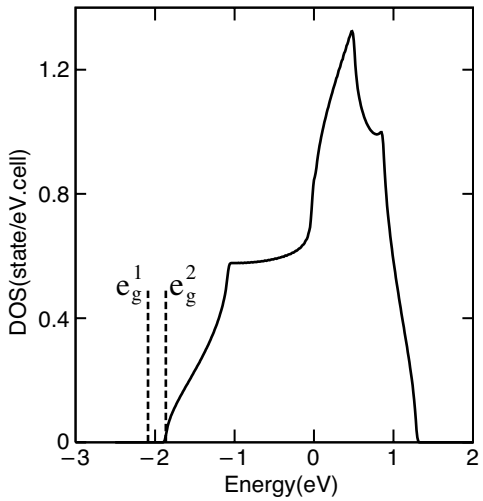

Figure 5. Illustration of the formation of the magnetic polaron state. The magnetic polaron states (dashed lines) form below the e_g bands in AF $CaMnO_3$, obtained by flipping a single t_{2g} spin (the central site) and thereby forming a seven-site FM cluster. The e_g states belonging to the central site spread over the seven-site FM region, reducing thereby their energies and producing two states below the band as shown. A first- and second-nearest-neighbour tight-binding model, with $t_{1NN} = -0.5$ eV and $t_{2NN} = -0.25$ eV, is used and neither are the spin angles optimized nor any lattice distortions allowed.

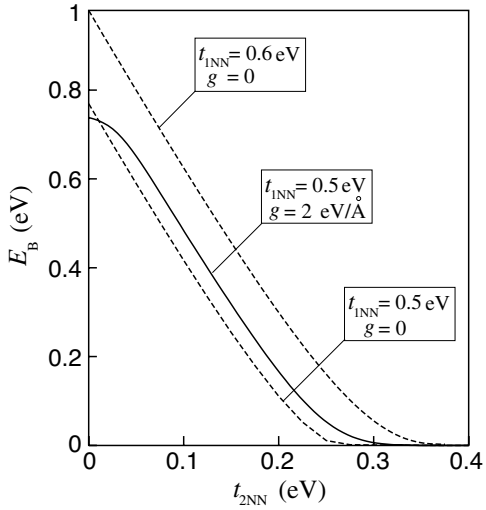

Figure 6. Binding energy of the magnetic polaron as a function of the second-nearest-neighbour hopping. Here $K = 10$ eV Å^{-2}.

where t_{1NN} is zero, leaving only a non-zero second-nearest-neighbour hopping in the lattice. In this case, even in the presence of an excess electron, the AF lattice is preferred, since the electron can hop everywhere in the lattice, while for the case with a ferromagnetic polaron region within the AF lattice, hopping between certain 2NNs are blocked because of the wrong spin alignment. Thus, both the electron kinetic energy and the superexchange between the

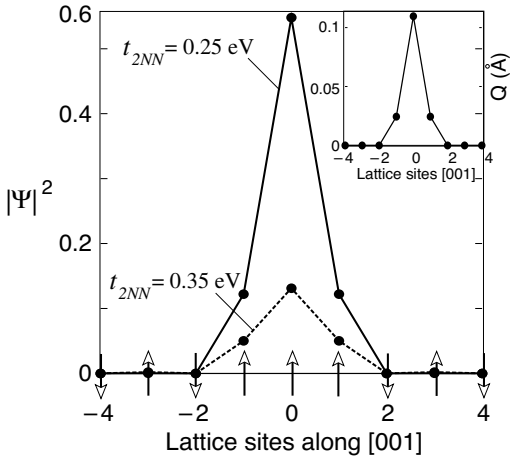

Figure 7. Wavefunction of the electron along the [001] direction of the simple cubic lattice for two different values of the second-nearest-neighbour hopping. The arrows represent the spin orientation of the t_{2g} lattice spins. The inset shows the magnitudes of the total lattice distortion $Q = (Q_2^2 + Q_3^2)^{1/2}$. Parameters are: $t_{1NN} = 0.6$ eV, $g = 2$ eV Å^{-1} and $K = 10$ eV Å^{-2}. For the inset, we also have $t_{2NN} = 0.25$ eV.

t_{2g} spins disfavour the formation of the magnetic polaron region. The excess electron is delocalized over the entire lattice, which remains antiferromagnetic, and no polaron region is formed.

When both the first- and second-nearest-neighbour hoppings are taken into account, there is a competition between them, with the 1NN term preferring an FM polaron region, while the 2NN hopping quickly destabilizes it in favour of a fully AF lattice. For a fixed t_{1NN}, there exists a critical magnitude for t_{2NN}, beyond which the FM polaron region does not form (figure 6). It turns out that for typical solids, the magnitude of t_{2NN} is large enough that the binding energy of the polaron is reduced by a substantial amount.

The Jahn–Teller coupling g was shown in section 2 to enhance the polaron energy, but only by a small amount, and this is also what we find from the full calculation (figure 6). Notice however that the polaron binding energy actually *diminishes* for $t_{2NN} = 0$ if the Jahn–Teller coupling g is present. This is so because, as remarked in section 2, the AF lattice has an especially large Jahn–Teller energy gain. And because all hopping is prohibited in the AF case, this is also the total energy, so that $E_{AF} = -g^2/2K$. In other words, the electron becomes localized on a single octahedron in the AF lattice, in order to take full advantage of the Jahn–Teller coupling. Thus the binding energy, which measures the energy of the FM polaron state with respect to that of the AF state, is actually lower if the Jahn–Teller coupling is present (compare the solid curve versus the dashed curve for $g = 2$ in figure 6 for $t_{2NN} = 0$). This case is however rare, and in general the Jahn–Teller coupling g does enhance the polaron binding energy, *albeit* by a small amount.

The wavefunction of the doped electron along the [001] direction is shown in figure 7. The total wavefunction shown is the sum of the contributions from both the $3z^2 - r^2$ and $x^2 - y^2$ orbitals. For the set of parameters chosen these two contributions are comparable in magnitude. The solid and dashed lines represent the total wavefunction of the electron for two different values of the nearest-neighbour hopping. For parameters appropriate for $CaMnO_3$, the wavefunction of the electron is localized to the central site, dropping rapidly away from the centre, forming a seven-site FM cluster configuration. As t_{2NN} is increased, it causes the

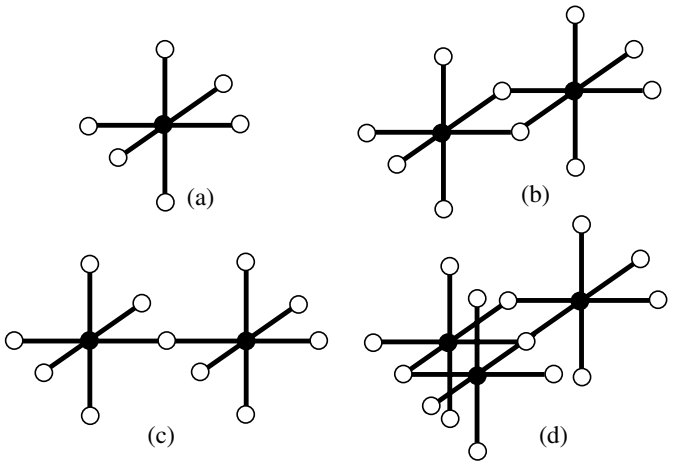

Figure 8. Some of the ferromagnetic clusters used as initial guesses in the total energy optimization. These are formed by flipping a few spins by 180° and are shown here because of their frequent proximity to the global minimum. In the text, we refer to these clusters as: (a) seven-site FM, (b) twelve-site FM, (c) thirteen-site FM, etc. Full circles indicate the Mn atoms with flipped spins, while the open circles indicate the Mn atoms with spins unchanged from the original antiferromagnetic lattice.

electron to spread more in the lattice, thus lowering the magnitude of its wavefunction on the central site, while simultaneously increasing it on sites away from the centre.

The inset in figure 7 shows the magnitude of the distortion $Q = (Q_2^2 + Q_3^2)^{1/2}$ of the lattice along the [001] direction. The distortion is very strong at the centre of the polaron and decreases rapidly away from the centre. This is to be expected in light of the fact that the magnitude of the Jahn–Teller distortion goes roughly as $(-g/K) \times \psi(r)^2$ ($\psi(r)$ is the electron wavefunction at the site r) as discussed in section 2.

5.3. Results for $La_{1-x}Ca_xMnO_3$

So far in our discussion, the ground-state polaron configuration corresponded to a seven-site FM cluster. There are however other possible spin configurations which may, depending on the parameters, have a lower energy than the seven-site configuration. Some of these configurations are shown in figure 8, chosen because of their proximity to the global minimum configuration.

Chen *et al* [12] also considered such clusters in their work; however, they did not proceed with a global minimization process, nor did they consider the second-nearest-neighbour hopping, which, as discussed above, are very important for the polaron problem.

Now, in order to form an FM cluster, one has to flip one or more t_{2g} spins, thus gaining NN hopping energy at the cost of NNN hopping. Therefore clusters with more than a few flipped spins are too expensive energetically. In addition to the AF type-G configuration, we choose four different spin configurations with one, two, or three spins flipped, and study the energetics of the polaron. The results for several different clusters are shown in figure 8.

Of all the clusters, the seven-site cluster has the lowest kinetic energy gain due to t_{1NN} (smaller electron confinement region), while the increase in energy due to blocking of the t_{2NN} hopping as well as due to the 'wrong' FM bonds is also low. For the thirteen-site cluster, all three terms are higher in magnitude. Since the t_{1NN} term competes against the other two, it is not clear which of these two or some other cluster would win ultimately. The energies for

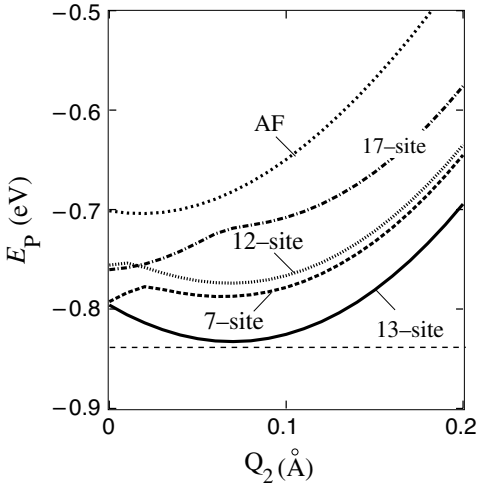

Figure 9. Energy of the magnetic polaron for different FM clusters as a function of the dominant lattice distortion mode Q_2 at the central Mn site. The dashed horizontal line corresponds to the global energy minimum. The parameters are $t_{1NN} = 0.5$ eV, $t_{2NN} = 0.2$ eV, $g = 2$ eV Å^{-1}, and $K = 10$ eV Å^{-2}.

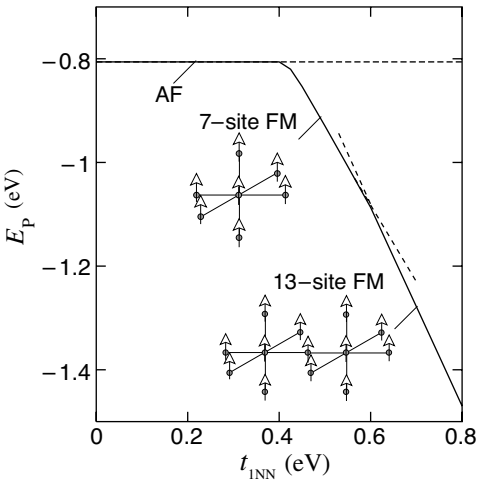

Figure 10. Total energy of the magnetic polaron showing a change in the minimum energy configuration from an AF to a seven-site and then to a thirteen-site FM cluster as t_{1NN} is varied. Note that below $t_{1NN} \approx 0.4$ eV, the antiferromagnetic lattice is stable and a polaron is not formed. The parameters are $t_{2NN} = 0.25$ eV, $g = 2$ eV Å^{-1}, and $K = 10$ eV Å^{-2}.

the various clusters are shown in figure 9, where, for the parameters chosen, the thirteen-site cluster wins.

We generally find that either the seven-site or the thirteen-site cluster has the minimum energy, when the polaron forms. Of course, the possibility is not excluded that in a different material some other cluster might be energetically favoured.

Note that because of the competition between the NN and the NNN hopping, the magnetic polaron is not always energetically favourable. This is clearly shown in figure 10, where the AF type-G is the lowest energy state for values of $t_{1NN} \lesssim 0.4$ eV.

5.4. Density-functional results

While the model results discussed above describe the physics of the magnetic polarons, for a quantitative calculation of the polaron binding energy, one must turn to more accurate methods. To this end, we have performed calculations using the density-functional theory (DFT), which takes account of the further neighbour interactions, hopping via oxygen atoms, as well as the finite magnitude of the Hund energy, all of which were approximated in our model.

A global optimization of the structure to obtain the spin angles and the lattice distortions at all sites in the solid is a horrendous task and is not particularly illuminating. However, our model calculations discussed above have given the following insights into the structure of the magnetic polaron.

(a) For a broad range of Hamiltonian parameters, the magnetic polaron consists of the seven-site (and sometimes the thirteen-site) FM region; of these, the experiments seem to favour the former.
(b) The t_{2g} lattice spins belonging to the seven-site cluster are completely ferromagnetic, while the rest of the lattice retains more or less the AF structure.

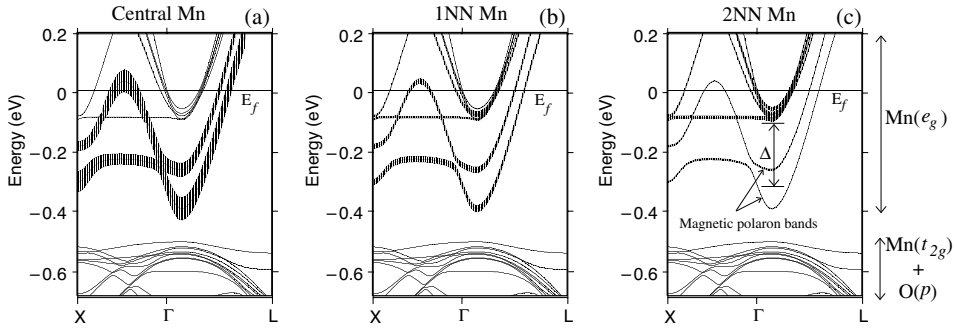

Figure 11. Supercell energy bands of $(La_{1/32}Ca_{31/32}MnO_3)_{32}$ obtained from the density-functional calculations [15] for the seven-site FM cluster with fixed t_{2g} lattice spins. The fat bands' thicknesses are proportional to the occupancy of the e_g electrons for the central Mn atom (a), the six 1NN Mn atoms (b), and the twelve 2NN Mn atoms (c). Notice the formation of the two 'magnetic polaron bands,' which drop down into the band gap of the undoped $CaMnO_3$, as was indicated also in figure 5. The energy Δ is indicative of the electron energy gain on account of delocalization into the seven-site FM region.

(c) The main distortion is of the Q_2-type on the central Mn site only, with the rest of the distortions being relatively small.

In light of this, we performed just two sets of density-functional calculations using the supercell technique, the supercell consisting of 32 formula units of $CaMnO_3$ with one Ca^{2+} replaced by La^{3+}. This introduces one doped electron per supercell into the conduction band and corresponds to an La doping of about 3%. Two separate magnetic calculations were performed: one for the type-G AF magnetic structure, and another where a central Mn(t_{2g}) spin was flipped, thus forming the seven-site FM cluster.

Since the only difference between the two structures in our calculations was the flipping of the spin of the central Mn atom without any relaxation of the atomic positions, the total energy difference is expected to be meaningful, even though the calculations were performed with the simpler LMTO-ASA method. To check the accuracy of the calculated total energy, we computed the binding energy of the magnetic polaron from either the total energy difference or from the energy of the magnetic polaron bands, which agreed to about 10%. Further details of the density-functional calculations have been described elsewhere [15].

The main feature of the band structure is the introduction of two bands in the gap, which are due to the formation of a magnetic polaron state in the band gap of $CaMnO_3$. The calculated binding energy from DFT was about 100 meV [15], which is of the same order of energy found from our simple model calculations. Furthermore, the wavefunction of the itinerant electron is shown to rapidly drop as one moves away from the centre of the magnetic polaron, as can be seen from figure 11, which again is consistent with results of our model calculations.

When the excess electron polarizes a seven-site cluster, the central t_{2g} spin will change from $S = -3/2$ to $+3/2$, which will contribute 6 μ_B to the magnetization. An additional 1 μ_B is due to the spin of the excess electron which will align with that of the central spin. Therefore, the expected value of the magnetization in the presence of the seven-site cluster is 7 μ_B. The calculated magnetic moment of the seven-site polaron cluster from density-functional theory was about 6.68 μ_B as compared to the experimental value of 8.4 ± 0.35 μ_B obtained from the magnetization measurements [1]. This agreement indicates that the polaron found in the experiment for $CaMnO_3$ is close to a seven-site structure. As mentioned above, we did not optimize the spin angles of the Mn atoms in the DFT calculations. This optimization would

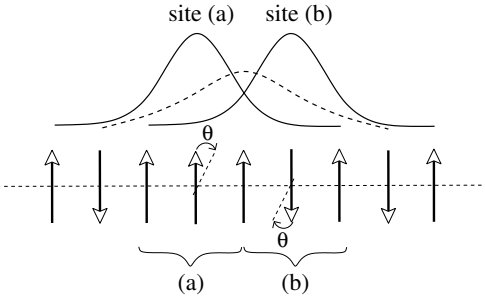

Figure 12. Illustrating a possible mechanism of activated hopping of the self-trapped magnetic polaron in one dimension. As the spin angle θ changes from zero to π, the three-site FM region has shifted from site (a) to site (b), with a resulting hopping of the electron. The dashed curve represents the electronic wavefunction for the intermediate state with $\theta = \pi/2$, during the hopping process.

indeed increase the magnetization of the polaron by canting the spins of the neighbouring sites parallel to the magnetization of the seven-site region.

5.5. Polaron conductivity

The measured conductivity of the magnetic polaron in the electron-doped manganites show an activated behaviour with an activation energy in the range of 30–95 meV [1]. The activated behaviour seems reasonable as one expects the conductivity for the magnetic polarons to be metallic with a renormalized effective mass in the large polaron limit, while the conductivity is expected to be activated type in the small polaron limit. In the latter case, as the electron moves from site to site, the lattice spins must turn so that the magnetic polaron region moves along with the electron.

In the small lattice polaron limit, the transport takes place via hopping of an electron from one site to another while it carries the lattice distortion along with it. In the process, the polaron must go through an intermediate configuration, necessarily of a higher energy. If the extra energy is lower than the typical energy of the optical phonon, then the lattice distortion can follow the process of the electron and no activation energy is necessary. For the opposite situation, it is hard for the lattice distortion to follow the electron transfer, and an activation energy is necessary [27]. Stoneham [28] reported a calculation of this activation energy by considering an intermediate state, putting half the charge of the electron on each of the two sites involved in the hopping process. A full lattice relaxation for the intermediate state is then carried out to compute E_A.

In the case of the magnetic polaron, we follow a similar line of reasoning, with the lattice distortion replaced by the exchange-induced distortion of the lattice spins. We imagine that the electron hopping takes place by an adiabatic process, where the lattice spins slowly rotate (see figure 12), with the electron following the spins adiabatically. Thus for each fixed position of the spin angle θ, we compute the total energy of the system by optimizing the electronic wavefunction.

For $CaMnO_3$, we consider the electron hopping from a seven-site magnetic polaron cluster to a neighbouring one, as shown in figure 13. The intermediate configuration is formed by turning two of the lattice spins by the angle π, as shown in the figure. Figure 13(b) shows the polaron energy as a function of the configuration coordinate θ with the parameters $t_{1NN} = 0.5$ eV, $t_{2NN} = 0.22$ eV, $g = 2$ eV Å^{-1}, $K = 10$ eV Å^{-2}, and $JS^2 = 5$ meV. The

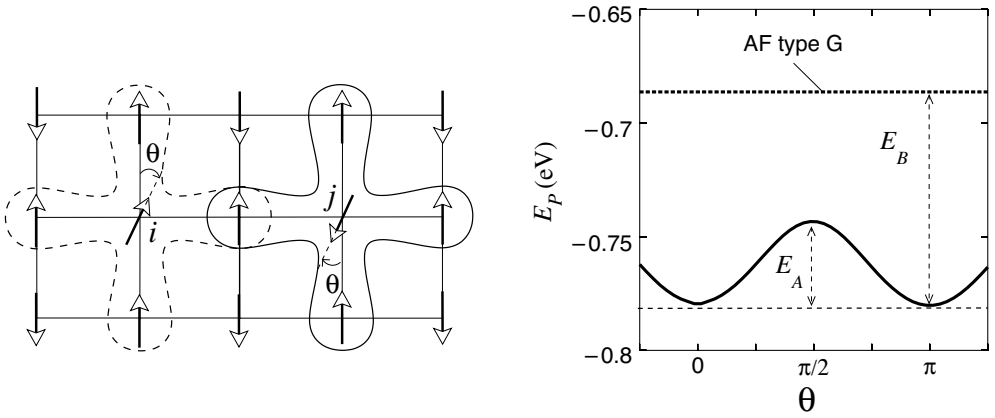

Figure 13. A mechanism for the hopping of the magnetic polaron between two sites by changing the spin angle θ continuously from zero to π (a). Notice that as the angle changes from zero to π, the centre of the seven-site FM polaron has shifted from site i to site j (polaron hopping). Figure (b) shows the corresponding polaron energy as a function of θ, showing the activation barrier E_{A}.

parameters were chosen so that the polaron binding energy is roughly the same as the result of the DFT calculation, i.e. about 100 meV. From figure 13, we find an activation energy of about 40 meV, of the same order of magnitude as the experimental result [1].

6. Conclusion

We have studied the problem of the self-trapped magnetic polaron in an antiferromagnetic lattice for the electron-doped manganites in the low doping limit using a model Hamiltonian that incorporates the various interaction terms. We found that the second-nearest-neighbour hopping has a crucial effect on the polaron energy, reducing the binding energy by a substantial amount and sometimes even destabilizing the polaron completely in favour of an antiferromagnetic state, while the Jahn–Teller interaction has a marginal effect. For parameters appropriate for $CaMnO_3$, the lattice spins formed a seven-site ferromagnetic cluster, in which the electron becomes self-trapped. A density-functional calculation for the seven-site ferromagnetic cluster yielded a polaron binding energy of about 100 meV, which is robust enough that it is unlikely to be washed away by effects such as the quantum fluctuations, whose effects are difficult to take into account in a realistic calculation.

We argued that the conductivity of the magnetic polaron is due to activated hopping, the activation energy coming from the path in the configuration space (necessarily of higher energy) that the polaron must take in the hopping process. The estimated activation energy is about 40 meV, which is the same order of magnitude as found in the experiments [1].

Finally, we emphasize that the present theory concerns a *single* doped electron in $CaMnO_3$, so that it is valid strictly in the limit $x \to 0$. When additional electrons are doped, it is possible that the magnetic polarons formed by the individual electrons would coalesce into ferromagnetic droplets. In fact, recent neutron scattering experiments suggest the formation of such droplets [29, 30]. However, in these experiments, in order to make the data consistent with the magnetization measurements, spin canted regions had to be hypothesized in addition to the droplets. On the other hand, such spin canted regions were not observed in the same experiments, nor have they been seen in any other experiments on the manganites to our knowledge, in spite of de Gennes' suggestion of it quite a long time ago [31]. Unfortunately,

the neutron scattering experiments were performed on polycrystalline samples, making it even more difficult to draw any firm conclusions. Thus, a clear picture of the magnetism in the low-doped $CaMnO_3$ is still an open question and awaits further experiments, preferably on single crystal samples, as well as further theoretical work on the formation of the polaron droplets.

Acknowledgments

We thank Dasgupta T S and Thulasi S for stimulating discussions. This work was supported in part by a grant from the Department of Energy under contract No DE-FG02-00E0045818.

References

[1] Neumeier J J and Cohn J L 2000 *Phys. Rev.* B **61** 14319
[2] Kasuya T, Yanase A and Takeda T 1970 *Solid State Commun.* **8** 1543
[3] Mott N F 1974 *Metal–Insulator Transitions* (London: Taylor and Francis)
[4] Nagaev E L 1971 *Sov. Phys.—Solid State* **34** 961
[5] Busch G *et al* 1964 *Phys. Lett.* **12** 11
[6] Arai T *et al* 1973 *J. Phys. Soc. Japan* **34** 68
[7] Demin R V, Koroleva L I and Balbashov A M 1999 *Pis. Zh. Eksp. Teor. Fiz.* **70** 303
[8] Oliveira N F, Foner S, Shapira Y and Reed T B 1972 *Phys. Rev.* B **5** 2634
[9] Shapira Y, Foner S, Oliveira N F and Reed T B 1972 *Phys. Rev.* B **5** 2647
[10] Wachter P 1970 *Solid State Commun.* **8** 473
[11] Von Molnar S and Methfessel S 1967 *J. Appl. Phys.* **38** 959
[12] Chen Y R and Alen P B 2001 *Phys. Rev.* B **64** 064401
[13] Pathak S and Satpathy S 2001 *Phys. Rev.* B **63** 214413
[14] Satpathy S and Popović Z S 2000 *Phys. Rev. Lett.* **84** 1603
[15] Meskine H, Saha-Dasgupta T and Satpathy S 2004 *Phys. Rev. Lett.* **92** 056401
[16] Saha-Dasgupta T and Satpathy S 2003 *J. Phys.: Condens. Matter* **15** 1685
[17] Van Vleck J H 1939 *J. Chem. Phys.* **7** 72
[18] Kanamori J 1960 *J. Appl. Phys.* **31** 14S
[19] Bersuker I B 1984 *The Jahn–Teller Effect and Vibronic Interactions in Modern Chemistry* (New York: Plenum)
[20] Kaplan M D and Vekhter B G 1995 *Cooperative Phenomena in Jahn–Teller Crystals* (New York: Plenum)
[21] Satpathy S, Popović Z S and Vukajlović F R 1996 *Phys. Rev. Lett.* **76** 960
[22] Anderson P W and Hasegawa H 1955 *Phys. Rev.* **100** 675
[23] Harrison W A 1980 *Electronic Structure and the Properties of Solids* (San Francisco, CA: Freeman)
[24] Rushbrooke J S and Wood P J 1958 *Mol. Phys.* **1** 257
[25] Rushbrooke J S and Wood P J 1963 *Mol. Phys.* **5** 409
[26] Fisher M E 1967 *Rep. Prog. Phys.* **30** 617
[27] Kasuya T and Yanase A 1968 *Rev. Mod. Phys.* **40** 684
[28] Stoneham A M 1989 *J. Chem. Soc. Faraday Trans.* 2 **85** 505 and references therein
[29] Ling C D *et al* 2003 *Phys. Rev.* B **68** 134439
[30] Granado E *et al* 2003 *Phys. Rev.* B **68** 134440
[31] de Gennes P-G 1960 *Phys. Rev.* **118** 141